

ON 3-PARAMETER FAMILIES OF PIECEWISE SMOOTH VECTOR FIELDS IN THE PLANE.

CLAUDIO A. BUZZI¹, TIAGO DE CARVALHO² AND
MARCO A. TEIXEIRA³

ABSTRACT. This paper is concerned with the local bifurcation analysis around typical singularities of piecewise smooth planar dynamical systems. Three-parameter families of a class of non-smooth vector fields are studied and the tridimensional bifurcation diagrams are exhibited. Our main results describe the unfolding of the so called *fold – cusp* singularity by means of the variation of 3 parameters.

1. INTRODUCTION

NSDS's have become certainly one of the common frontiers between Mathematics and Physics or Engineering. Problems involving impact or friction are piecewise-smooth, as are many control systems with thresholds. Many authors have contributed to the study of Filippov systems (see for instance [7] and [10]). One of the starting points for a systematic approach to the geometric and qualitative analysis of non-smooth dynamical systems (NSDS's, for short) is [13], on smooth systems in 2-dimensional manifolds with boundary. The generic singularities that appear in NSDS's, to the best of our knowledge, were first studied in [15]. Bifurcations and related problems involving or not sliding regions were studied in papers like [6, 8, 2, 3]. The classification of codimension-1 local and some global bifurcations for planar systems was given in [11]. In [9] codimension-2 singularities were discussed and it was shown how to construct the homeomorphisms which lead to topological equivalences between two NSDS's when the discontinuity set is a planar smooth curve. See [16] or [4] for a survey on NSDS's and references there in.

The specific topic addressed in this paper is the qualitative analysis of *fold–cusp singularities* of NSDS's, where a fold and a cusp coincide. Moreover, the bifurcation diagrams are exhibited.

Specifically, we distinguish the following cases (see Figure 1):

2010 *Mathematics Subject Classification.* Primary 34A36, 37G10, 37G05.

Key words and phrases. non-smooth vector field, bifurcation, canard cycle, limit cycle, pseudo equilibrium.

- Unfolding of an invisible fold–cusp singularity:

$$(1) \quad Z_{\lambda, \beta, \mu} = \begin{cases} X_\lambda = \begin{pmatrix} 1 \\ -x + \lambda \end{pmatrix} & \text{if } y \geq 0, \\ Y_\beta = \begin{pmatrix} -1 \\ -x^2 + \beta - \frac{\partial B}{\partial x}(x, \beta, \mu) \end{pmatrix} & \text{if } y \leq 0, \end{cases}$$

where $(\lambda, \beta) \in (-\lambda_0, \lambda_0) \times (-\beta_0, \beta_0)$, with $\lambda_0 > 0$ and $\beta_0 > 0$ sufficiently small and B is a C^2 -bump function such that $B(x, \beta, \mu) = 0$ if $\beta \leq 0$ and

$$(2) \quad B(x, \beta, \mu) = \begin{cases} 0, & \text{if } x < -\sqrt{\beta} \text{ or } x > 4\sqrt{\beta}; \\ B_1(x, \beta) + f(\beta, \mu), & \text{if } -\sqrt{\beta} \leq x \leq \sqrt{\beta}; \\ B_2(x, \beta) + f(\beta, \mu), & \text{if } \sqrt{\beta} < x \leq 4\sqrt{\beta}. \end{cases}$$

if $\beta > 0$, where

$$B_1(x, \beta) = \frac{-3}{128\beta} \left(\frac{x^2(208 + 3\beta) - 4x\sqrt{\beta}(176 + 15\beta) + \beta(688 + 93\beta)}{128\beta} \right),$$

$$B_2(x, \beta) = \frac{-1}{48\beta} \left(\frac{(x - 4\sqrt{\beta})^3((x^2 + \beta)(-16 + 9\beta) - 2x\sqrt{\beta}(16 + 15\beta))}{48\beta} \right)$$

and

$$f(\beta, \mu) = \frac{\mu}{48} \left(\frac{-8\beta(128 + 3\beta)\mu\sqrt{\beta}(256 + 63\beta)\mu - (-64 + 45\beta)\mu^2 - \beta^{-1/2}(80 + 3\beta)\mu^3 + \beta^{-1}(-16 + 9\beta)\mu^4}{48} \right).$$

- Unfolding of a visible fold–cusp singularity:

$$(3) \quad Z_{\lambda, \beta} = \begin{cases} X_\lambda = \begin{pmatrix} 1 \\ x - \lambda \end{pmatrix} & \text{if } y \geq 0, \\ Y_\beta = \begin{pmatrix} 1 \\ -x^2 + \beta \end{pmatrix} & \text{if } y \leq 0, \end{cases}$$

where $(\lambda, \beta) \in (-\lambda_0, \lambda_0) \times (-\beta_0, \beta_0)$, with $\lambda_0 > 0$ and $\beta_0 > 0$ sufficiently small.

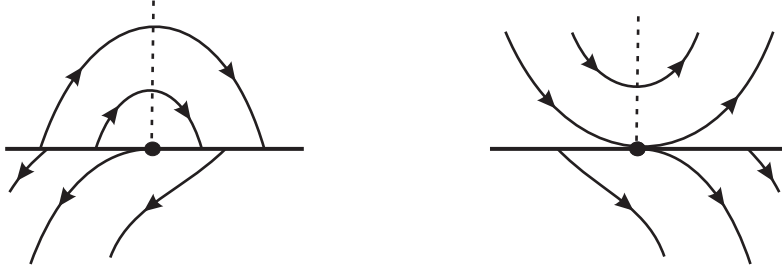


FIGURE 1. Fold–cusp singularities. Following the notation of [9], a point $p_0 \in \Sigma$ is a **fold–cusp singularity** of $Z = (X, Y)$ if it is a Σ -fold point of X and a Σ -cusp point of Y (see precise definitions in Section 2).

1.1. Setting the problem. Denote both, $Z_{\beta,\lambda,\mu}$ in (1) and $Z_{\beta,\lambda}$ in (3), by $Z = (X, Y)$. In short our goal is to study the local dynamics of Z consisting of two smooth vector fields X and Y in \mathbb{R}^2 such that on one side of a smooth surface $\Sigma = \{y = 0\}$ we take $Z = X$ and on the other side $Z = Y$.

In [9] the analysis of the bifurcation diagram of the 2-parameter family

$$W_{\mu,\epsilon} = \begin{cases} X_\mu = \begin{pmatrix} 1 \\ x - \mu \end{pmatrix} & \text{if } y \geq 0, \\ Y_\epsilon = \begin{pmatrix} -1 \\ -x^2 + \epsilon \end{pmatrix} & \text{if } y \leq 0. \end{cases}$$

of NSDS's presenting an invisible fold-cusp singularity is performed. A challenging problem is to extend the analysis of [9] in answering the following question: Can we find families of NSDS's presenting fold-cusp singularities whose dynamics is richer than the family exhibited in [9]? In this paper such an extension has been carried out. By means of the positive answer to the previous question, we are able to say that two parameters is not enough to explain the birth of some new topological types around $Z_{0,0,0}$.

In fact, our results cover the study done in [9] and we can obtain the bifurcation diagram presented in [9] assuming $\beta = \mu^2$ and $\mu \leq 0$ in (1). For example, the configuration in Figure 2 is not observed in [9] and is present at the bifurcation diagram of (1).

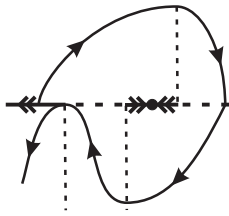


FIGURE 2. Configuration nearby $Z_{0,0,0}$ not observed in [9].

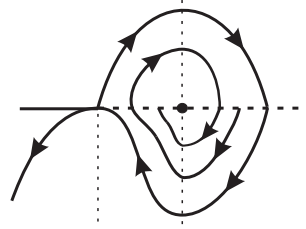


FIGURE 3. The local and the global bifurcation observed in (1) when $\beta > 0$, $\lambda = \sqrt{\beta}$ and $\mu = 0$.

We mention two particular situations illustrated in Figure 3 that occur in (1) when $\beta > 0$. In this *resonant* configuration we note, simultaneously, a two-fold singularity (which is a local phenomenon) and a loop passing through the visible Σ -fold of Y (which is a global phenomenon).

1.2. Statement of the Main Results. Theorems 1, 2 and 3 pave the way for the proof of Theorem A. Theorem B is self contained.

Theorem 1. *If $\mu = 0$ in Equation (1) then its bifurcation diagram in the (λ, β) -plane contains essentially 17 distinct phase portraits (see Figure 23).*

It is easy to see that the cases covered by Theorem 1 do not represent the full unfolding of the invisible fold–cusp singularity. Because of this, the next two theorems are necessary.

Theorem 2. *If $0 < \mu < \mu_0$ in Equation (1) then its bifurcation diagram in the (λ, β) –plane contains essentially 19 distinct phase portraits (see Figure 25).*

Theorem 3. *If $-\mu_0 < \mu < 0$ in Equation (1) then its bifurcation diagram in the (λ, β) –plane contains essentially 19 distinct phase portraits (see Figure 25).*

Finally, we are in position to state the main results of the paper.

Theorem A. *The bifurcation diagram of Equation (1) exhibits 55 distinct cases representing 23 distinct phase portraits (see Figure 27).*

Theorem B. *The bifurcation diagram of Equation (3) exhibits 11 distinct phase portraits (see Figure 33).*

The paper is organized as follows. In Section 2 we present some basic elements on the theory of NSDS's. In Sections 3, 4 and 5 we pave the way for the proofs of the main results of the paper (Theorems A and B). Section 6 is devoted to prove Theorem A and exhibit the Bifurcation Diagram of (1). In Section 7, the proof of Theorem B and the Bifurcation Diagram of (3) are presented and in Section 8 some concluding remarks are discussed. In our paper we follow basically the terminology and the approach of [11] or [9] and no one sophisticated tool is needed.

2. PRELIMINARIES

Let $K \subseteq \mathbb{R}^2$ be a compact set such that ∂K is a smooth 1–manifold and $\Sigma \subseteq K$ given by $\Sigma = f^{-1}(0)$, where $f : K \rightarrow \mathbb{R}$ is a smooth function having $0 \in \mathbb{R}$ as a regular value (i.e. $\nabla f(p) \neq 0$, for any $p \in f^{-1}(0)$) such that $\partial K \cap \Sigma = \emptyset$ or $\partial K \pitchfork \Sigma$. Clearly the *switching manifold* Σ is the separating boundary of the regions $\Sigma^+ = \{q \in K | f(q) \geq 0\}$ and $\Sigma^- = \{q \in K | f(q) \leq 0\}$.

Designate by χ the space of C^1 –vector fields on K endowed with the C^1 –topology. Call $\Omega = \Omega(K, f)$ the space of vector fields $Z : K \rightarrow \mathbb{R}^2$ such that

$$(4) \quad Z(x, y) = \begin{cases} X(x, y), & \text{for } (x, y) \in \Sigma^+, \\ Y(x, y), & \text{for } (x, y) \in \Sigma^-, \end{cases}$$

where $X = (f_1, g_1)$, $Y = (f_2, g_2)$ are in χ . We write $Z = (X, Y)$, which we will accept to be multivalued in points of Σ . We endow Ω with the product C^1 -topology. The trajectories of Z are solutions of $\dot{q} = Z(q)$, which has, in general, discontinuous righthand side. The basic results of differential equations, in this context, were stated by Filippov in [7].

Definition 1. A k -parameter family of elements in Ω is a C^1 -mapping, with $r > 1$,

$$\begin{aligned} \zeta : S^k &\longrightarrow \Omega \\ \varrho = (\varrho_1, \varrho_2, \dots, \varrho_k) &\mapsto X_\varrho \end{aligned}$$

where $S^k = [-\epsilon_1, \epsilon_1] \times [-\epsilon_2, \epsilon_2] \times \dots \times [-\epsilon_k, \epsilon_k]$ with $\epsilon_i > 0$, $i = 1, 2, \dots, k$, sufficiently small.

Definition 2. We say that $W, \tilde{W} \in \chi$ defined in open sets U and \tilde{U} , respectively, are \mathbf{C}^0 -orbitally equivalent if there exists an orientation preserving homeomorphism $h : U \rightarrow \tilde{U}$ that sends orbits of W to orbits of \tilde{W} . Here, orbit of W means the image of a solution of $\dot{x} = W(x)$.

Definition 3. Two non-smooth vector fields $Z = (X, Y)$, $\tilde{Z} = (\tilde{X}, \tilde{Y}) \in \Omega(K, f)$ defined in open sets $U, \tilde{U} \subset K$ and with switching manifold Σ are Σ -equivalent if there exists an orientation preserving homeomorphism $h : U \rightarrow \tilde{U}$ that sends Σ in Σ , the orbits of X restrict to $U \cap \Sigma^+$ in the orbits of \tilde{X} restrict to $\tilde{U} \cap \Sigma^+$, and the orbits of Y restrict to $U \cap \Sigma^-$ in the orbits of \tilde{Y} restrict to $\tilde{U} \cap \Sigma^-$.

Consider the notation

$$X.f(p) = \langle \nabla f(p), X(p) \rangle \quad \text{and} \quad X^i.f(p) = \langle \nabla X^{i-1}.f(p), X(p) \rangle, i \geq 2$$

where $\langle \cdot, \cdot \rangle$ is the usual inner product in \mathbb{R}^2 .

Remark 1. The vertical dotted lines present in almost all figures of this paper represent the points $p \in K \subset \mathbb{R}^2$ where $X.f(p) = 0$ or $Y.f(p) = 0$

We distinguish the following regions on the discontinuity set Σ :

- (i) $\Sigma^c \subseteq \Sigma$ is the *sewing region* if $(X.f)(Y.f) > 0$ on Σ^c .
- (ii) $\Sigma^e \subseteq \Sigma$ is the *escaping region* if $(X.f) > 0$ and $(Y.f) < 0$ on Σ^e .
- (iii) $\Sigma^s \subseteq \Sigma$ is the *sliding region* if $(X.f) < 0$ and $(Y.f) > 0$ on Σ^s .

Consider $Z \in \Omega$. The *sliding vector field* associated to Z is the vector field Z^s tangent to Σ^s and defined at $q \in \Sigma^s$ by $Z^s(q) = m - q$ with m being the point of the segment joining $q + X(q)$ and $q + Y(q)$ such that $m - q$ is tangent to Σ^s (see Figure 4). It is clear that if $q \in \Sigma^s$ then $q \in \Sigma^e$ for $-Z$ and then we can define the *escaping vector field* on Σ^e associated to Z by $Z^e = -(-Z)^s$. In what follows we use the notation Z^Σ for both cases.

We say that $q \in \Sigma$ is a Σ -regular point if

- (i) $(X.f(q))(Y.f(q)) > 0$ or

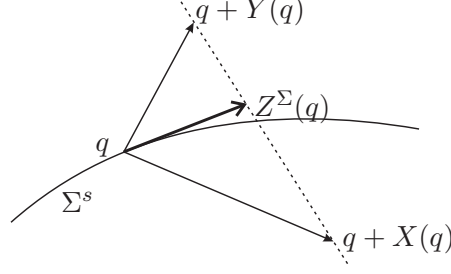


FIGURE 4. Filippov's convention.

- (ii) $(X.f(q))(Y.f(q)) < 0$ and $Z^\Sigma(q) \neq 0$ (that is $q \in \Sigma^e \cup \Sigma^s$ and it is not an equilibrium point of Z^Σ).

The points of Σ which are not Σ -regular are called Σ -singular. We distinguish two subsets in the set of Σ -singular points: Σ^t and Σ^p . Any $q \in \Sigma^p$ is called a *pseudo equilibrium* of Z and it is characterized by $Z^\Sigma(q) = 0$. Any $q \in \Sigma^t$ is called a *tangential singularity* and is characterized by $Z^\Sigma(q) \neq 0$ and $(X.f(q))(Y.f(q)) = 0$ (q is a contact point).

We say that a point $p_0 \in \Sigma$ is a Σ -fold point of X if $X.f(p_0) = 0$ but $X^2.f(p_0) \neq 0$. Moreover, $p_0 \in \Sigma$ is a *visible* (respectively *invisible*) Σ -fold point of X if $X.f(p_0) = 0$ and $X^2.f(p_0) > 0$ (respectively $X^2.f(p_0) < 0$). We say that a point $q_0 \in \Sigma$ is a Σ -cusp point of Y if $Y.f(q_0) = Y^2.f(q_0) = 0$ and $Y^3.f(q_0) \neq 0$. Moreover, a Σ -cusp point q_0 of Y is of *kind 1* (respectively *kind 2*) if $Y^3.f(q_0) > 0$ (respectively $Y^3.f(q_0) < 0$). In particular, Σ -fold and Σ -cusp points are tangential singularities.

A pseudo equilibrium $q \in \Sigma^p$ is a Σ -saddle provided that one of the following conditions is satisfied: (i) $q \in \Sigma^e$ and q is an attractor for Z^Σ or (ii) $q \in \Sigma^s$ and q is a repeller for Z^Σ . A pseudo equilibrium $q \in \Sigma^p$ is a Σ -repeller (resp. Σ -attractor) provided $q \in \Sigma^e$ (respectively $q \in \Sigma^s$) and q is a repeller (respectively, attractor) equilibrium point for Z^Σ .

Given a point $q \in \Sigma^c$, we denote by $r(q)$ the straight line through $q + X(q)$ and $q + Y(q)$.

Definition 4. The Σ -regular points $q \in \Sigma^c$ such that either $\{X(q), Y(q)\}$ is a linearly dependent set or $r(q) \cap \Sigma = \emptyset$ are called **virtual pseudo equilibria**.

Let us consider a smooth autonomous vector field W defined in an open set U . Then we denote its flow by $\phi_W(t, p)$. In this way,

$$\begin{cases} \frac{d}{dt}\phi_W(t, p) = W(\phi_W(t, p)), \\ \phi_W(0, p) = p, \end{cases}$$

where $t \in I = I(p, W) \subset \mathbb{R}$, an interval depending on $p \in U$ and W .

The following definition was stated in [9], pg 1971.

Definition 5. The *local trajectory* of a NSDS given by (4) is defined as follows:

- For $p \in \Sigma^+$ and $p \in \Sigma^-$ the trajectory is given by $\phi_Z(t, p) = \phi_X(t, p)$ and $\phi_Z(t, p) = \phi_Y(t, p)$ respectively, where $t \in I$.
- For $p \in \Sigma^c$ such that $X.f(p) > 0$, $Y.f(p) > 0$ and taking the origin of time at p , the trajectory is defined as $\phi_Z(t, p) = \phi_Y(t, p)$ for $t \in I \cap \{t \leq 0\}$ and $\phi_Z(t, p) = \phi_X(t, p)$ for $t \in I \cap \{t \geq 0\}$. For the case $X.f(p) < 0$ and $Y.f(p) < 0$ the definition is the same reversing time.
- For $p \in \Sigma^e \cup \Sigma^s$ such that $Z^\Sigma(p) \neq 0$ we define $\phi_Z(t, p) = \phi_{Z^\Sigma}(t, p)$ for $t \in I$.
- For $p \in \partial\Sigma^c \cup \partial\Sigma^e \cup \partial\Sigma^s$ such that the definitions of trajectories for points in a full neighborhood of p in Σ can be extended to p and coincide, the trajectory through p is this trajectory.
- For any other point $\phi_Z(t, p) = p$ for all $t \in \mathbb{R}$. This is the case of points in $\partial\Sigma^c \cup \partial\Sigma^e \cup \partial\Sigma^s$ which are not regular tangential singularities and the equilibrium points of X in Σ_+ , of Y in Σ_- and of Z^Σ in $\Sigma^s \cup \Sigma^e$.

Definition 6. The *local orbit-arc* of the vector field W passing through a point $p \in U$ is the set $\gamma_W(p) = \{\phi_W(t, p) : t \in I\}$.

Since we are dealing with autonomous systems, from now on we will use trajectory and orbit-arc indistinctly when there is no danger of confusion.

Definition 7. Consider $Z = (X, Y) \in \Omega$.

- (1) A *canard cycle* is a closed curve $\Gamma = \bigcup_{i=1}^n \sigma_i$ composed by the union

of orbit-arcs σ_i , $i = 1, \dots, n$, of $X|_{\Sigma^+}$, $Y|_{\Sigma^-}$ and Z^Σ such that:

- Either there exists $i_0 \subset \{1, \dots, n\}$ with $\sigma_{i_0} \subset \gamma_X$ (respectively $\sigma_{i_0} \subset \gamma_Y$) and then there exists $j \neq i_0$ with $\sigma_j \subset \gamma_Y \cup \gamma_{Z^\Sigma}$ (respectively $\sigma_j \subset \gamma_X \cup \gamma_{Z^\Sigma}$), or Γ is composed by a single arc σ_i of Z^Σ ;
- the transition between arcs of X and arcs of Y occurs in sewing points;
- the transition between arcs of X (or Y) and arcs of Z^Σ occurs through Σ -fold points or regular points in the escaping or sliding arc, respecting the orientation. Moreover if $\Gamma \neq \Sigma$ then

there exists at least one visible Σ -fold point on each connected component of $\Gamma \cap \Sigma$.

(2) A canard cycle Γ of Z is of:

- **Kind I** if Γ meets Σ just in sewing points;
- **Kind II** if $\Gamma = \Sigma$;
- **Kind III** if Γ contains at least one visible Σ -fold point of Z .

In Figures 5, 6 and 7 arise canard cycles of kind I, II and III respectively.

(3) A canard cycle Γ of Z is **hyperbolic** if one of the following conditions are satisfied:

- (i) Γ is of kind I and $\eta'(p) \neq 1$, where η is the first return map defined on a segment T with $p \in T \pitchfork \gamma$;
- (ii) Γ is of kind II;
- (iii) Γ is of kind III, $\overline{\Sigma^e} \cap \overline{\Sigma^s} \cap \Gamma = \emptyset$ and either $\Gamma \cap \Sigma \subseteq \Sigma^c \cup \Sigma^e \cup \Sigma^t$ or $\Gamma \cap \Sigma \subseteq \Sigma^c \cup \Sigma^s \cup \Sigma^t$.

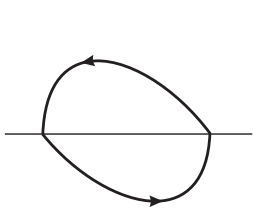


FIGURE
5. Canard
cycle of
kind I.

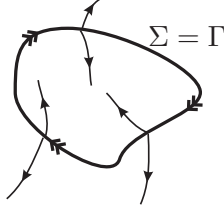


FIGURE
6. Canard
cycle of
kind II.

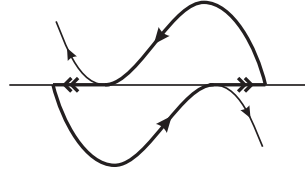


FIGURE
7. Canard
cycle of kind
III.

Following Theorem 2 of [17], locally it is possible to consider $f(x, y) = y$ and conclude that any $X \in \Sigma^+$ presenting a Σ -fold point is C^0 -orbitally equivalent to the normal form $X_0(x, y) = (\rho_1, \rho_2 x)$ with $\rho_1 = \pm 1$ and $\rho_2 = \pm 1$.

Following [13], we can take $f(x, y) = y$ and derive that any $Y \in \Sigma^-$ presenting a Σ -cusp point is C^0 -orbitally equivalent to the normal form $Y_0(x, y) = (\rho_3, \rho_4 x^2)$ with $\rho_3 = \pm 1$ and $\rho_4 = \pm 1$.

Lemma 8. *Let $Z = (X, Y) \in \Omega$ presenting a fold-cusp singularity, then Z is Σ -equivalent to the standard form $Z_0 = Z_{\rho_1, \rho_2, \rho_3, \rho_4}$ given by*

$$(5) \quad Z_\rho = Z_{\rho_1, \rho_2, \rho_3, \rho_4} = \begin{cases} X_{\rho_1, \rho_2} = \begin{pmatrix} \rho_1 \\ \rho_2 x \end{pmatrix} & \text{if } y \geq 0, \\ Y_{\rho_3, \rho_4} = \begin{pmatrix} \rho_3 \\ \rho_4 x^2 \end{pmatrix} & \text{if } y \leq 0 \end{cases}$$

where $\rho_1, \rho_2, \rho_3, \rho_4 = \pm 1$.

Observe that the values of ρ_i , $i = 1, 2, 3, 4$, in Lemma 8 depend on the orientation of X and Y . In Subsection 2.3 we prove Lemma 8, i.e., we exhibit the homeomorphism that characterizes the equivalence between any fold–cusp singularity and the standard form given by (5).

Consider $Z_0^{ivb,k1}, Z_0^{vis,k2} \in \Omega$ written in the following standard forms (similar forms were stated in Section 12 of [9]):

$$(6) \quad Z_0^{ivb,k1} = \begin{cases} X_0^{ivb} = \begin{pmatrix} 1 \\ -x \end{pmatrix} & \text{if } y \geq 0, \\ Y_0^{k1} = \begin{pmatrix} -1 \\ -x^2 \end{pmatrix} & \text{if } y \leq 0, \text{ and} \end{cases}$$

$$(7) \quad Z_0^{vis,k2} = \begin{cases} X_0^{vis} = \begin{pmatrix} 1 \\ x \end{pmatrix} & \text{if } y \geq 0, \\ Y_0^{k2} = \begin{pmatrix} 1 \\ -x^2 \end{pmatrix} & \text{if } y \leq 0. \end{cases}$$

Note that X_0^{ivb} presents an invisible Σ –fold point on its phase portrait, X_0^{vis} presents a visible Σ –fold point, Y_0^{k1} presents a Σ –cusp point of kind 1 and Y_0^{k2} presents a Σ –cusp point of kind 2. Moreover, in (6) we made $\rho_1 = 1$ and $\rho_2 = \rho_3 = \rho_4 = -1$ in (5) and in (7) we made $\rho_1 = \rho_2 = \rho_3 = 1$ and $\rho_4 = -1$ in (5). For simplicity we restrict our study to the normal forms given above, i.e, (6) and (7). All the other choices on the values of ρ_i , $i = 1, 2, 3, 4$ in (5) are treated similarly.

The main problem is to exhibit the bifurcation diagram of $Z_0^{\tau,\rho}$ where $\tau = ivb$ or vis and $\rho = k1$ or $k2$.

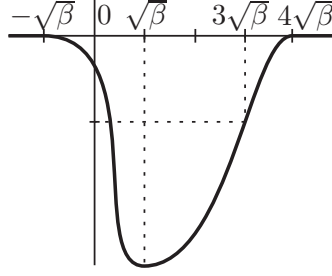
In order to detect a larger range of topological behaviors near an invisible fold–cusp singularity we have to refine the analysis done in [9]. This refinement can be obtained adding a bump function on the expression of the NSDS.

Denote

$$F(x) = \int g_2(x, \beta, \mu) dx = \frac{x^3}{3} - \beta x + B(x, \beta, \mu) + c_0,$$

where $c_0 = -2\beta\sqrt{\beta}/3$ and g_2 is the second coordinate of $Y_{\beta,\mu}$ in (1). The C^1 –bump function B satisfies the following properties when $\beta > 0$:

- It has exactly one point of local minimum in the interval $(-\sqrt{\beta}, 4\sqrt{\beta})$. This point is located at $x_0 = \sqrt{\beta}$.
- $F(3\sqrt{\beta} + \mu) = 0$ (see Figure 8). By means of this last property the orbit–arc of $Y_{\beta,\mu}$ that has a quadratic contact to Σ at $q_0 = (-\sqrt{\beta}, 0)$ turns to collide with Σ at the point $q_1 = (3\sqrt{\beta} + \mu, 0)$. So, the first coordinate of q_1 is bigger (respectively, smaller) than $3\sqrt{\beta}$ as μ is bigger (respectively, smaller) than 0.

FIGURE 8. Graph of B .

Remark 2. *It is worth saying that the parameter μ breaks the strong proportionality between the roots of $g_2(x, \beta, 0)$. At the limit value $\mu_0 = 0$, $Z_{\lambda, \beta, \mu}$ presents distinct topological behaviors for $\mu < \mu_0$ or $\mu > \mu_0$.*

Remark 3. *Note that in Equations (1) and (3) the perturbations considered depend only on the variable x . The local geometry of a NSDS presenting a cusp–fold singularity becomes rather different if perturbations involving the variables x and y are admitted.*

2.1. Global Bifurcation. As said before, the configuration illustrated in Figure 3 plays a very important role in our analysis. The configuration of this figure is reached from (1), by taking $\beta > 0$, $\lambda = \sqrt{\beta}$ and $\mu = 0$. In this section we deal with this global phenomenon.

Emphasizing, let $Z_0 = (X_0, Y_0) \in \Omega$ having the following properties:

- The discontinuity set Σ is represented by $f(x, y) = y$.
- Consider $X_0 = (f_1^0, g_1^0)$ and $Y_0 = (f_2^0, g_2^0)$ and assume that $f_1^0(p) > 0$ if $p \in \Sigma^+$ and $f_2^0(p) < 0$ if $p \in \Sigma^-$.
- $q_0 \in \Sigma$ is a visible Σ –fold point of Y_0 and $X.f(q_0) > 0$.
- The orbit $\gamma_{X_0}(q_0)$ of X_0 through q_0 meets transversally Σ at a point q_1 .
- The orbit $\gamma_{Y_0}(q_1)$ of Y_0 through q_1 meets tangentially Σ at q_0 . Call Γ the degenerate canard cycle composed by $\gamma_{X_0}(q_0)$ and $\gamma_{Y_0}(q_1)$. Let M be the compact region in the plane bounded by Γ .

2.1.1. Transition Fold Map. As $q_0 \in \Sigma$ is a visible Σ –fold point of Y_0 , we may assume (see [17]) coordinates around q_0 such that the system is represented by $(\dot{x}, \dot{y}) = (-1, x)$ with $q_0 = (0, 0)$. The solutions of this differential equation are given by:

$$\phi_{a,b}(t) = (-t + a, -(t^2/2) + at + b).$$

The orbit–arc ϕ_0 through $(0, 0)$ is represented by $\phi_0(t) = (-t, -t^2/2)$.

Let δ be a very small positive number. We construct the *Transition Map* $\xi : L_1 \rightarrow L_0$, from $L_1 = \{(x, y), y = -\delta, x \geq \sqrt{2\delta}\}$ to $L_0 = \{(x, 0), x \geq 0\}$, following the orbits of Y_0 (see Figure 9). The curve L_1 is transverse to

Y_0 at $p_\delta = (\sqrt{2\delta}, -\delta)$. Since the solutions ϕ_δ through $(\bar{x}, -\delta) \in L_1$ meet $\Sigma = \{y = 0\}$ at time $t = \bar{x} \pm \sqrt{\bar{x}^2 - 2\delta}$ we obtain that $\xi(\bar{x}) = \sqrt{\bar{x}^2 - 2\delta}$ and ξ is an homeomorphism. Moreover, $\xi^{-1}(x) = \sqrt{x^2 + 2\delta}$, ξ^{-1} is differentiable at 0 and $(\xi^{-1})'(0) = 0$.

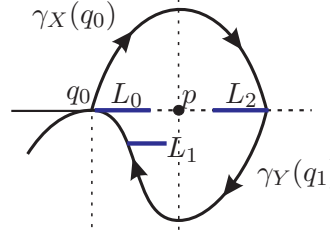


FIGURE 9. First Return Map around the two-fold singularity p .

2.1.2. First Return Map associated to Γ . Let ϱ_X be the transition map from L_0 to $L_2 \subset \Sigma$ via X_0 -trajectories and ϱ_Y be the transition map from L_2 to L_1 via Y_0 -trajectories (see Figure 9). Observe that the linear part of the composition $\varrho_Y \circ \varrho_X$ is nonzero due to the transversality conditions of the problem. For simplicity, let $J_\epsilon = [0, \epsilon) \times \{0\}$ be a small semi-open interval of Σ .

So the First Return Map of Z_0 at q_0 is $\kappa(x) = (\xi \circ \varrho_Y \circ \varrho_X)(x)$ for $x \in J_\epsilon$. Its inverse κ^{-1} is a differentiable map at 0 and satisfies $(\kappa^{-1})'(0) = 0$. So, Γ locally repels the orbits of Z_0 closed to Γ and in the interior of Γ .

In conclusion, if Z is very close to Z_0 in Ω in such a way that it possesses a canard cycle nearby Γ then it is a hyperbolic repeller canard cycle. Under some other conditions on Z_0 (reversing the directions of X_0 and Y_0) we can derive that such canard cycle is an attractor.

2.1.3. Analysis around the two-fold singularity. In Equation (1), for $\beta > 0$, it is possible to define a *First Return Map* $\psi_\lambda^\mu : (\sqrt{\beta}, 3\sqrt{\beta} + \mu) \rightarrow (\sqrt{\beta}, 3\sqrt{\beta})$, associated to $Z_{\lambda, \beta, \mu}$, given by

$$\psi_\lambda^\mu(x) = (\varrho_{X_\lambda} \circ \varrho_{Y_{\mu, \beta}})(x)$$

where $\varrho_{Y_{\mu, \beta}}(x)$ is the first return to Σ of the orbit-arc of $Y_{\mu, \beta}$ that passes through $p = (x, 0)$ and $\varrho_{X_\lambda}(\tilde{x})$ is the first return to Σ of the orbit-arc of X_λ that passes through $p = (\tilde{x}, 0)$.

Lemma 9. *If $\beta > 0$, $\lambda = \sqrt{\beta}$ and $\mu = 0$ in (1) then (see Figure 3) the First Return Map $\psi_\lambda^\mu(x)$ satisfies*

- (i) $\psi_\lambda^0(x) < x$, $\forall x \in (\sqrt{\beta}, 3\sqrt{\beta})$ and
- (ii) $|(\psi_\lambda^0)'(\sqrt{\beta})| \neq 1$.

Proof. Consider Figure 9. Given a point $p \in L_2$, the positive Y -orbit by p reaches L_3 at the point $q = (q_1, q_2)$ and the negative X -orbit by p reaches

L_0 at the point $\tilde{p} = (\tilde{p}_1, \tilde{p}_2)$. The negative Y -orbit by \tilde{p} reaches L_3 at the point $\tilde{q} = (\tilde{q}_1, \tilde{q}_2)$. Since

$$q_2 - \tilde{q}_2 = \frac{(p_1 - 3\sqrt{\beta})(p_1 - \sqrt{\beta})^3(p_1(1744 + 99\sqrt{\beta}) - \sqrt{\beta}(6256 + 321\beta))}{384\beta}$$

and $\sqrt{\beta} < p_1 < 3\sqrt{\beta}$ we conclude that $q_2 - \tilde{q}_2 > 0$ and item (i) is proved. Item (ii) follows from Section 2.1.2. \square

Note that Lemma 9 implies that $Z_{\sqrt{\beta}, \beta, 0}$ does not have closed orbits in the interior of the closed curve of Z passing through the visible Σ -fold point of $Y_{0, \beta}$. Moreover, when $\mu < 0$ (see Figure 10), Lemma 9 guarantees that ψ_λ^μ has a unique fixed point \bar{x} where $\bar{x} < 3\sqrt{\beta} + \mu$. And, in this case, $|(\psi_\lambda^\mu)'(\bar{x})| \neq 1$, i.e., \bar{x} is a hyperbolic fixed point for ψ_λ^μ that corresponds to a hyperbolic canard cycle of $Z_{\lambda, \beta, \mu}$. When $\mu > 0$ (see Figure 10), $\psi_\lambda^\mu(x) < x$ for all $x \in (\sqrt{\beta}, 3\sqrt{\beta} + \mu)$ and closed orbits of $Z_{\lambda, \beta, \mu}$ do not arise.

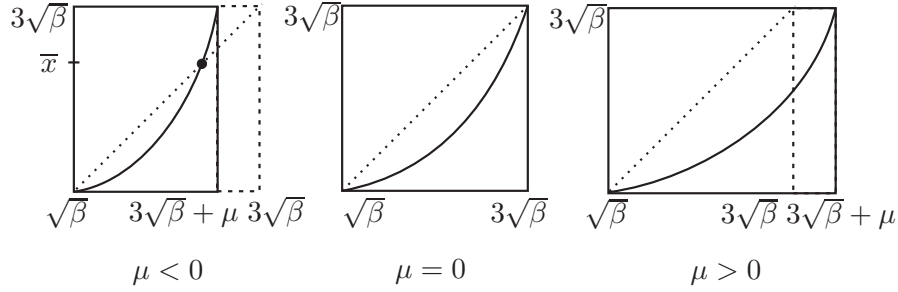


FIGURE 10. Graph of the First Return Map ψ_λ^μ .

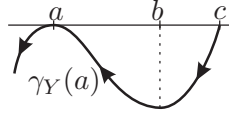
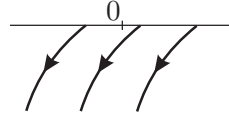
Given $Z = (X, Y)$, we describe some properties of both $X = X_\lambda$ and either $Y = Y_{\beta, \mu}$ or $Y = Y_\beta$.

The parameter λ measures how the Σ -fold point $d = (\lambda, 0)$ of X is translated away from the origin. More specifically, if $\lambda < 0$ then d is translated to the left hand side and if $\lambda > 0$ then d is translated to the right hand side.

The parameter β distinguishes the contact order between a trajectory of Y and Σ . In this way, it occurs one, and only one, of the following situations:

- \mathbf{Y}^+ : In this case $\beta > 0$. So Y has two Σ -fold points in such a way that one of them is invisible and the other one is visible. These points are expressed by $a = a_\beta = (-\sqrt{\beta}, 0)$ and $b = b_\beta = (\sqrt{\beta}, 0)$. Moreover, a third point $c = c_{\beta, \mu} = (3\sqrt{\beta} + \mu, 0)$ plays an important role at the analysis of (1). This point is the locus where the orbit-arc $\gamma_Y(a)$ intersects transversally Σ for negative time (see Figure 11). Using the bump function B the distance between c and b is bigger or smaller than the distance between a and b according to the value of the parameter μ . This fact will be important to change from Theorem 1 to Theorems 2 and 3.

- \mathbf{Y}^0 : In this case $\beta = 0$. So Y has a Σ -cusp point $e = (0, 0)$ (see Figure 1).
- \mathbf{Y}^- : In this case $\beta < 0$. So Y does not have Σ -fold points. In this way, $Y.f \neq 0$ and Y is transversal to Σ (see Figure 12).

FIGURE 11. Case Y^+ .FIGURE 12. Case Y^- .

2.2. The Direction Function. The next function will be very useful in the sequel.

On Σ , consider the point $C = (C_1, C_2)$, the vectors $X(C) = (D_1, D_2)$ and $Y(C) = (E_1, E_2)$ (as illustrated in Figure 13). Observe that the straight line $r(C)$ by $q + X(q)$ and $q + Y(q)$, generically, meets Σ in a point $p(C)$. We define the C^r -map

$$\begin{aligned} p: \Sigma &\longrightarrow \Sigma \\ z &\longmapsto p(z). \end{aligned}$$

We choose local coordinates such that Σ is the x -axis; so $C = (C_1, 0)$ and $p(C) \in \mathbb{R} \times \{0\}$ can be identified with points in \mathbb{R} . According with this identification, the *direction function* on Σ is defined by

$$\begin{aligned} H: \mathbb{R} &\longrightarrow \mathbb{R} \\ z &\longmapsto p(z) - z. \end{aligned}$$

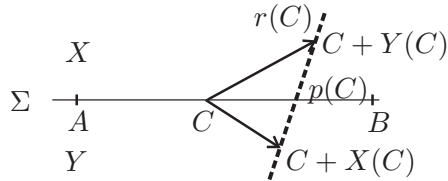


FIGURE 13. Direction function.

Remark 4. We obtain that H is a C^r -map. When $C \in \Sigma^e \cup \Sigma^s$ the following holds:

- if $H(C) < 0$ then the orientation of Z^Σ in a small neighborhood of C is from B to A ;
- if $H(C) = 0$ then $C \in \Sigma^p$;
- if $H(C) > 0$ then the orientation of Z^Σ in a small neighborhood of C is from A to B .

Simple calculations show that $p(C_1) = \frac{E_2(D_1+C_1)-D_2(E_1+C_1)}{E_2-D_2}$ and consequently,

$$(8) \quad H(C_1) = \frac{E_2 D_1 - D_2 E_1}{E_2 - D_2}.$$

Remark 5. If $X.f(p) = 0$ and $Y.f(p) \neq 0$ then, in a neighborhood V_p of p in Σ , holds $H(V_p)D_1 > 0$, where $X(p) = (D_1, D_2)$. In fact, $X.f(p) = 0$ and $Y.f(p) \neq 0$ are equivalent to say that $D_2 = 0$ and $E_2 \neq 0$ in (8). So, $\lim_{(D_2, E_2) \rightarrow (0, k_0)} H(p_1) = D_1$, where $k_0 \neq 0$ and $p = (p_1, p_2)$.

Considering the previous notation and identifying Σ with the x -axis, we have that $r(C) \cap \Sigma = \emptyset$ when $E_2 = D_2$. In such a case, H is not defined at C . The following property is immediate.

Proposition 10. If n_1 is the number of pseudo equilibria and n_2 is the number of virtual pseudo equilibria then $n_1 + n_2 = v_1 + v_2$ where v_1 is the number of zeros of H and v_2 is the number of points q of Σ such that $r(q) \cap \Sigma = \emptyset$.

Proof. Straightforward according to Remark 4, Equation (8) and Definition 4. □

Remark 6. Given $Z_{\lambda, \beta, \mu}$, we list some properties of the function H . According to (8) we have that the expression of H is

$$H(x, \lambda, \beta, \mu) = \frac{H_1(x, \lambda, \beta, \mu)}{H_2(x, \lambda, \beta, \mu)}$$

where $H_1(x, \lambda, \beta, \mu) = -x^2 - x + \lambda + \beta - \frac{\partial B}{\partial x}(x, \beta, \mu)$ and $H_2(x, \lambda, \beta, \mu) = -x^2 + x - \lambda + \beta - \frac{\partial B}{\partial x}(x, \beta, \mu)$. So,

- (i) When $x = \lambda$ we get $H_1(\lambda, \lambda, \beta, \mu) = H_2(\lambda, \lambda, \beta, \mu)$.
- (ii) For the parameter values satisfying $\beta = \lambda^2 + \frac{\partial B}{\partial x}(\lambda, \beta, \mu) > 0$ we have $H_1(\lambda, \lambda, \beta, \mu) = H_2(\lambda, \lambda, \beta, \mu) = 0$.
- (iii) Since $H_1(0, 0, 0, 0) = 0$ (respectively $H_2(0, 0, 0, 0) = 0$) and $\frac{\partial H_1}{\partial x}(0, 0, 0, 0) = -1$ (respectively $\frac{\partial H_2}{\partial x}(0, 0, 0, 0) = 1$), by the Implicit Function Theorem there is a unique $x = x_{H_1}(\lambda, \beta, \mu)$ such that $H_1(x_{H_1}(\lambda, \beta, \mu), \lambda, \beta, \mu) = 0$ (respectively $H_2(x_{H_2}(\lambda, \beta, \mu), \lambda, \beta, \mu) = 0$). Therefore, there is only one zero of H_1 and only one zero of H_2 in a sufficiently small neighborhood of $x = 0$. These points are called p_1 and r_1 , respectively, in Figure 14. The pseudo equilibrium p_1 and the virtual pseudo equilibrium r_1 are the unique roots of H_1 and H_2 , respectively, that are relevant to our analysis. In fact, the other roots are far from the origin.

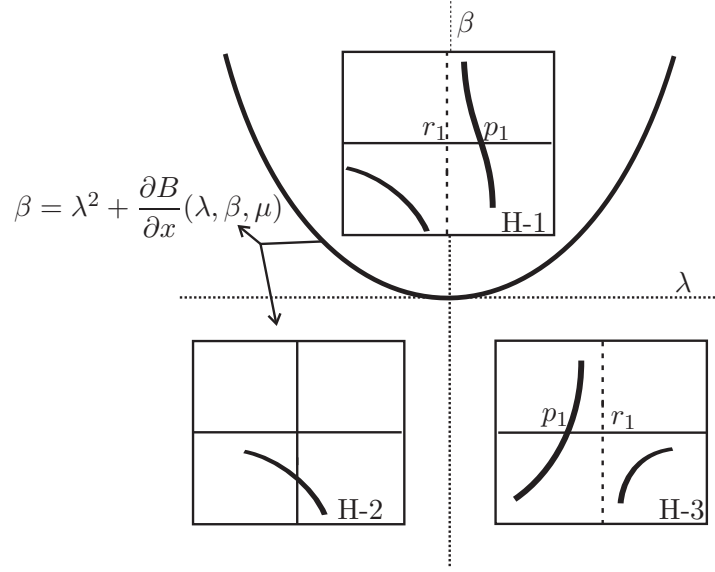


FIGURE 14. Variation of H with respect to λ and β . The dark lines in the boxes H-1, H-2 and H-3 correspond to the graph of H .

2.3. Proof of Lemma 8.

Now we prove Lemma 8.

Proof of Lemma 8. Here we construct a Σ -preserving homeomorphism h that sends orbits of $Z = (X, Y)$ to orbits of $\tilde{Z} = (\tilde{X}, \tilde{Y})$, where $\tilde{Z} = Z_\rho$ is given by (5) with $\rho_1 = 1$ and $\rho_i = -1$, $i = 2, 3, 4$. The other choices on parameters ρ_i , $i = 1, 2, 3, 4$, are treated in a similar way. Let p (respectively, \tilde{p}) be the fold-cusp singularity of Z (respectively, \tilde{Z}) (see Figure 15). Identify p with \tilde{p} , i.e., $h(p) = \tilde{p}$. Consider a point $q \in \gamma$ (respectively, $\tilde{q} \in \tilde{\gamma}$),

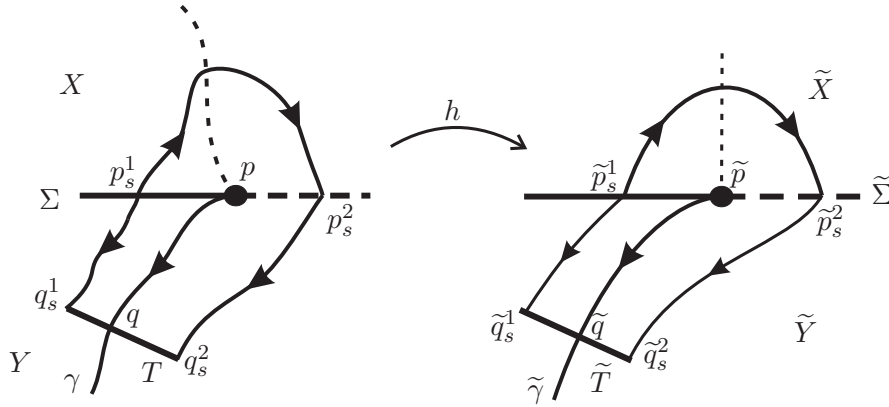


FIGURE 15. Construction of the homeomorphism.

where γ (respectively, $\tilde{\gamma}$) is the orbit–arc of Y (respectively, \tilde{Y}) starting at p (respectively, \tilde{p}). Identify γ with $\tilde{\gamma}$ (i.e., $h(\gamma) = \tilde{\gamma}$) from a reparametrization by arc–length. Let T (respectively, \tilde{T}) be transversal sections to Y (respectively, \tilde{Y}) passing through q (resp., \tilde{q}) with small amplitude. Identify T with \tilde{T} (i.e., $h(T) = \tilde{T}$) by arc–length. Let $q_s^1 \in T$ be a point on the left of q . Using the Implicit Function Theorem (abbreviated by IFT), there exists a time $t_s^1 < 0$, depending on q_s^1 , such that $\phi_Y(q_s^1, t_s^1) := p_s^1 \in \Sigma$. Since $h(T) = \tilde{T}$, there exists $\tilde{q}_s^1 \in \tilde{T}$ such that $h(q_s^1) = \tilde{q}_s^1$. Using IFT, there exists a time $\tilde{t}_s^1 < 0$, depending on \tilde{q}_s^1 , such that $\phi_{\tilde{Y}}(\tilde{q}_s^1, \tilde{t}_s^1) := \tilde{p}_s^1 \in \tilde{\Sigma}$. Identify the orbit–arc $\sigma_{q_s^1}^{p_s^1}(Y)$ of Y joining p_s^1 to q_s^1 with the orbit–arc $\tilde{\sigma}_{\tilde{q}_s^1}^{\tilde{p}_s^1}(\tilde{Y})$ of \tilde{Y} joining \tilde{p}_s^1 to \tilde{q}_s^1 (i.e., $h(\sigma_{q_s^1}^{p_s^1}(Y)) = \tilde{\sigma}_{\tilde{q}_s^1}^{\tilde{p}_s^1}(\tilde{Y})$) by arc–length. Fix the notation for the orbit–arcs of a given vector field joining two points. Since p (respectively, \tilde{p}) is a Σ –fold point of X (respectively, \tilde{X}), using the IFT, there exists a time $t_s^2 > 0$ (respectively, $\tilde{t}_s^2 > 0$), depending on p_s^1 (respectively, \tilde{p}_s^1), such that $\phi_X(p_s^1, t_s^2) := p_s^2 \in \Sigma$ (respectively, $\phi_{\tilde{X}}(\tilde{p}_s^1, \tilde{t}_s^2) := \tilde{p}_s^2 \in \tilde{\Sigma}$). Identify $\sigma_{p_s^1}^{p_s^2}(X)$ with $\tilde{\sigma}_{\tilde{p}_s^1}^{\tilde{p}_s^2}(\tilde{X})$ (i.e., $h(\sigma_{p_s^1}^{p_s^2}(X)) = \tilde{\sigma}_{\tilde{p}_s^1}^{\tilde{p}_s^2}(\tilde{X})$) by arc–length. Using the IFT, there exists a time $t_s^3 > 0$ (respectively, $\tilde{t}_s^3 > 0$), depending on p_s^2 (respectively, \tilde{p}_s^2), such that $\phi_Y(p_s^2, t_s^3) := q_s^2 \in T$ (resp., $\phi_{\tilde{Y}}(\tilde{p}_s^2, \tilde{t}_s^3) := \tilde{q}_s^2 \in \tilde{T}$). Identify $\sigma_{p_s^2}^{q_s^2}(Y)$ with $\tilde{\sigma}_{\tilde{p}_s^2}^{\tilde{q}_s^2}(\tilde{Y})$ (i.e., $h(\sigma_{p_s^2}^{q_s^2}(Y)) = \tilde{\sigma}_{\tilde{p}_s^2}^{\tilde{q}_s^2}(\tilde{Y})$) by arc–length.

So, the homeomorphism h sends Σ to $\tilde{\Sigma}$ and sends orbits of Z to orbits of \tilde{Z} . □

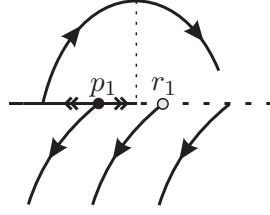
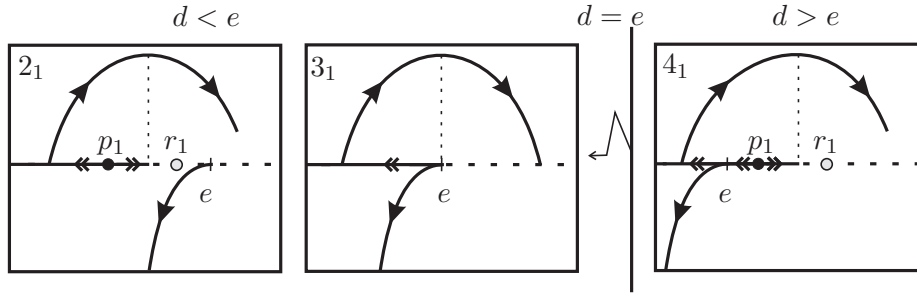
3. PROOF OF THEOREM 1

Proof of Theorem 1. In Case 1_1 we assume that Y presents the behavior Y^- where $\beta < 0$. In Cases 2_1 , 3_1 and 4_1 we assume that Y presents the behavior Y^0 where $\beta = 0$. In these cases canard cycles do not arise (for a proof, see [5]).

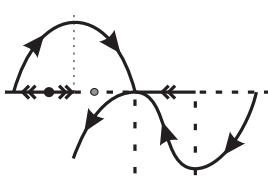
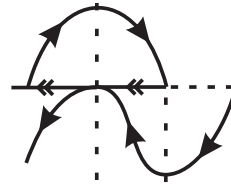
◊ *Case 1_1 . $\beta < 0$:* The points of Σ on the left of d belong to Σ^e and the points on the right of d belong to Σ^c . See Figure 16. Since $\beta < 0$, the graph of H is illustrated in H-3 of Figure 14. We get that $p_1 = (-1 + \sqrt{1 + 4\beta + 4\lambda}/2, 0) \in \Sigma^e$ is a Σ –repeller and $r_1 = (1 - \sqrt{1 + 4\beta - 4\lambda}/2, 0) \in \Sigma^c$.

◊ *Case 2_1 . $\lambda < 0$, Case 3_1 . $\lambda = 0$ and Case 4_1 . $\lambda > 0$:* The configuration of the connected components of Σ is the same as Case 1_1 . Since $\beta = 0$, the graph of H , when $\lambda \neq 0$, is given by H-3 of Figure 14. When $\lambda = 0$ (Case 3_1), the graph of H is given by H-2 of Figure 14 and $p_1 = r_1$. These cases are illustrated in Figure 17.

In Cases $5_1 - 17_1$ we assume that Y presents the behavior Y^+ where $\beta > 0$.

FIGURE 16. Case 1₁.FIGURE 17. Cases 2₁, 3₁ and 4₁.

◇ *Case 5₁*. $\lambda < -\sqrt{\beta}$: The points of Σ on the left of d belong to Σ^c , the points inside the interval (a, b) belong to Σ^s and the points on (d, a) and on the right of b belong to Σ^c . The graph of H is like H-3 of Figure 14. We can prove that p_1 is a Σ -repeller situated on the left of d and $r_1 \in (d, a)$. canard cycles do not arise. See Figure 18.

FIGURE 18. Case 5₁.FIGURE 19. Case 6₁.

◇ *Case 6₁*. $\lambda = -\sqrt{\beta}$: In this case the points on the right of b belong to Σ^c , the points on $(a = d, b)$ belong to Σ^s and the points on the left of $a = d$ belong to Σ^e . Since $\beta = \lambda^2$, H is like H-2 of Figure 14 and $p_1 = r_1$. There exists a non hyperbolic canard cycle Γ of kind III passing through a and c . See Figure 19.

◇ *Case 7₁*. $-\sqrt{\beta} < \lambda < 0$, *Case 8₁*. $\lambda = 0$ and *Case 9₁*. $0 < \lambda < \sqrt{\beta}$: The configuration of the connected components of Σ is like Case 5₁ replacing a by d and vice-versa. The graph of H is like H-1 of Figure 14. We observe

that $p_1 \in (d, b)$ is a Σ -attractor and $r_1 \in (a, d)$. There exists a hyperbolic repeller canard cycle Γ of kind III passing through a and c . See Figure 20.

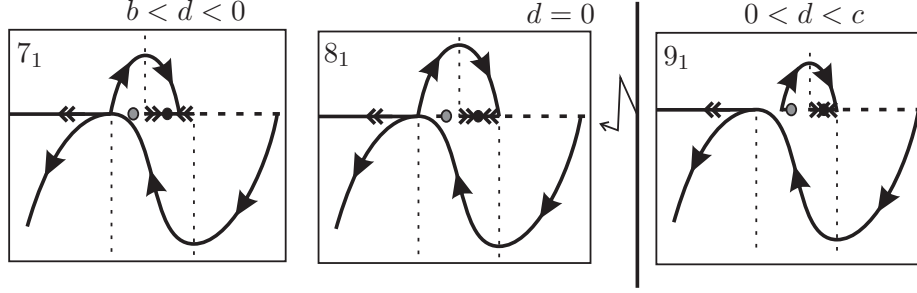


FIGURE 20. Cases $7_1 - 9_1$.

◇ *Case 10₁*. $\lambda = \sqrt{\beta}$: In this case the points on the left of a belong to Σ^e and the points on the right of a belong to Σ^c , except by $Q = (b, 0) \in \Sigma$. Since $\beta = \lambda^2$, H is like H-2 of Figure 14 and $p_1 = r_1$. Since $\mu = 0$ and $d = b$, by the construction of the bump function B it is straightforward to show that the point Q behaves itself like a weak attractor for Z and there exists a non hyperbolic canard cycle of kind III passing through a and c . See Figure 3. This case has already been discussed previously in Subsection 2.1. Note that in [9] the authors avoid this case.

◇ *Case 11₁*. $\sqrt{\beta} < \lambda < L_1$: The meaning of the value L_1 will be given below in this case. The points of Σ on the left of a and on (b, d) belong to Σ^e . The points on (a, b) and on the right of d belong to Σ^c . The graph of H is like H-3 of Figure 14. We can prove that $p_1 \in (b, d)$ is a Σ -repeller and r_1 is on the right of d . Since the point Q of the previous case is a weak attractor, in a neighborhood of d occurs a *Like Hopf Bifurcation*. Moreover, according to Lemma 9, there is a unique canard cycle Γ_1 in a neighborhood of d and a unique canard cycle Γ_2 in a neighborhood of c . Observe that both are of kind I, Γ_1 is attractor, Γ_2 is repeller and Γ_1 is located within the region bounded by Γ_2 . See Figure 21. Note that, as λ increases, Γ_1 becomes bigger and Γ_2 becomes smaller. When λ assumes the limit value L_1 , one of them collides with the other.

◇ *Case 12₁*. $\lambda = L_1$: The distribution of the connected components of Σ and the behavior of H are the same as Case 11₁. Since $\lambda = L_1$, as described in the previous case, there exists a non hyperbolic canard cycle Γ of kind I which is an attractor for the trajectories inside it and is a repeller for the trajectories outside it. See Figure 21.

◇ *Case 13₁*. $L_1 < \lambda < 2\sqrt{\beta}$, *Case 14₁*. $\lambda = 2\sqrt{\beta}$, *Case 15₁*. $2\sqrt{\beta} < \lambda < 3\sqrt{\beta}$, *Case 16₁*. $\lambda = 3\sqrt{\beta}$ and *Case 17₁*. $\lambda > 3\sqrt{\beta}$: The distribution of the connected components of Σ and the behavior of H are the same as Case 11₁. Canard cycles do not arise. See Figure 22.

The Bifurcation Diagram is illustrated in Figure 23. □

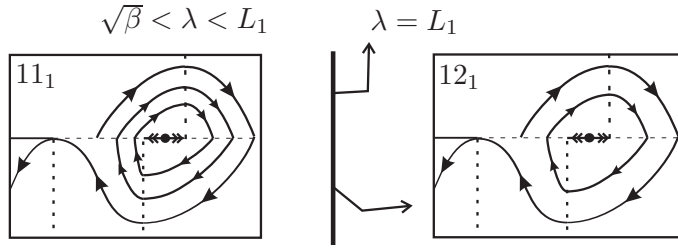
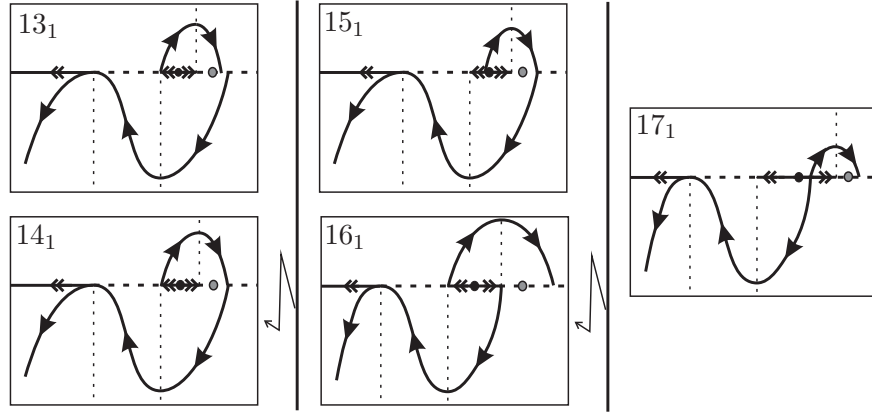
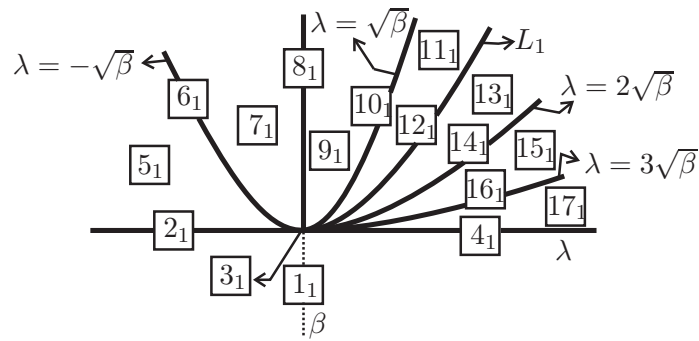
FIGURE 21. Cases 11_1 and 12_1 .FIGURE 22. Cases $13_1 - 17_1$.

FIGURE 23. Bifurcation Diagram of Theorem 1.

Remark 7. In Cases 9_1 and 11_1 the ST-bifurcations (as described in [9], Subsections 11.2 and 12.2) arise. In fact, note that the trajectory passing through a , in Case 9_1 , and c , in Case 11_1 , can make more and more turns

around p_1 . This fact characterizes a global bifurcation also reached in other cases.

4. PROOF OF THEOREM 2

Proof of Theorem 2. In Case 1_2 we assume that Y presents the behavior Y^- . In Cases $2_2, 3_2$ and 4_2 we assume that Y presents the behavior Y^0 . In Cases $5_2 - 19_2$ we assume that Y presents the behavior Y^+ .

◊ *Case 1_2 .* $\beta < 0$, *Case 2_2 .* $\lambda < 0$, *Case 3_2 .* $\lambda = 0$, *Case 4_2 .* $\lambda > 0$. *Case 5_2 .* $\lambda < -\sqrt{\beta}$. *Case 6_2 .* $\lambda = -\sqrt{\beta}$. *Case 7_2 .* $-\sqrt{\beta} < \lambda < 0$ and *Case 8_2 .* $\lambda = 0$: By the choice of the bump function B , these cases are analogous to Cases $1_1, 2_1, 3_1, 4_1, 5_1, 6_1, 7_1$ and 8_1 .

◊ *Case 9_2 .* $0 < \lambda < \sqrt{\beta} - \mu/2$: The analysis of this case is done in a similar way as the Case 9_1 . In this case and in Cases 7_2 and 8_2 there exists a hyperbolic repeller canard cycle Γ of kind III passing through a and c .

◊ *Case 10_2 .* $\lambda = \sqrt{\beta} - \mu/2$: The points of Σ on the left of a belong to Σ^e and the points on (d, b) belong to Σ^s . The points on (a, d) and on the right of b belong to Σ^c . The graph of H is like H-3 of Figure 14. Observe that $p_1 \in (d, b)$ is a Σ -attractor and r_1 is on the right of b . In this case the arc $\gamma_X(a)$ of X passing through a returns to Σ at the point c . So, in this case there arises a non hyperbolic canard cycle $\Gamma = \gamma_X(a) \cup \gamma_Y(c)$. By the discussion on subsection 2.1.2, we have that Γ is a repeller and we do not have other canard cycles inside Γ . See Figure 24.

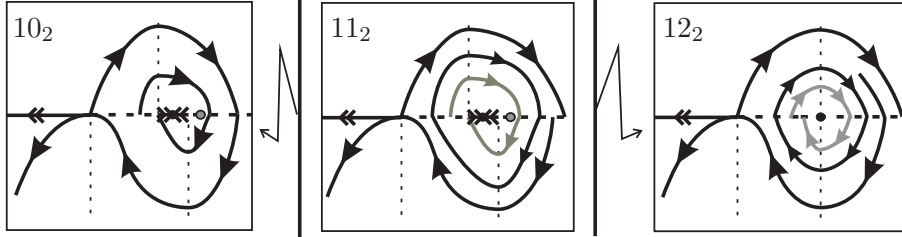


FIGURE 24. Cases $10_2 - 12_2$.

◊ *Case 11_2 .* $\sqrt{\beta} - \mu/2 < \lambda < \sqrt{\beta}$: The configuration on Σ and the graph of H are the same as Case 10_2 . Since $\varrho_X^{-1}(c) \in (a, d)$ there exists a point $Q \in (\varrho_X^{-1}(c), \varrho_X^{-1}(b))$ such that $\eta'(Q) = 1$. So there exists a hyperbolic repeller canard cycle Γ , of kind I, passing through Q . See Figure 24. Moreover, by Lemma 9 this canard cycle is unique. In Figure 10 we introduce the point \bar{x} which plays the same role of Q .

◊ *Case 12_2 .* $\lambda = \sqrt{\beta}$: The points of Σ on the left of a belong to Σ^e and the points on the right of a belong to Σ^c , except by the tangential singularity $c = d$. The graph of H is like H-2 of Figure 14. The repeller canard cycle Γ presented in the previous case is persistent. Recall that this canard cycle is born from the bifurcation of Case 10_2 . So, the radius of Γ does not tend

to zero when λ tends to $\sqrt{\beta}$. Moreover, the tangential singularity $b = d$ behaves itself like a weak attractor. See Figure 24.

◊ *Case 13₂*. $\sqrt{\beta} < \lambda < L_1$, *Case 14₂*. $\lambda = L_1$, *Case 15₂*. $L_1 < \lambda < 2\sqrt{\beta} + \mu/2$, *Case 16₂*. $\lambda = 2\sqrt{\beta} + \mu/2$, *Case 17₂*. $2\sqrt{\beta} + \mu/2 < \lambda < 3\sqrt{\beta} + \mu$, *Case 18₂*. $\lambda = 3\sqrt{\beta} + \mu$ and *Case 19₂*. $\lambda > 3\sqrt{\beta} + \mu$: The analysis of these cases is done in a similar way as Cases 11₁, 12₁, 13₁, 14₁, 15₁, 16₁ and 17₁, respectively.

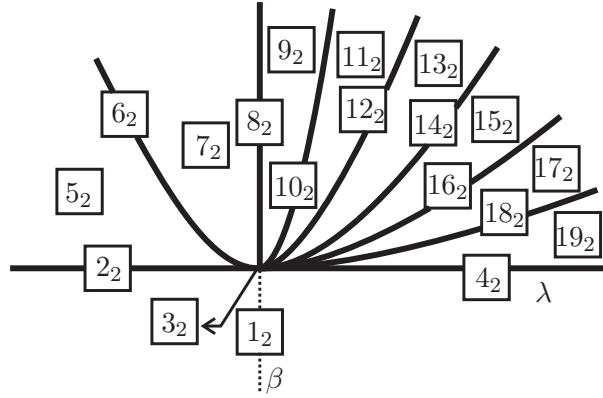


FIGURE 25. Bifurcation Diagram of Theorems 2 and 3.

The bifurcation diagram is illustrated in Figure 25. □

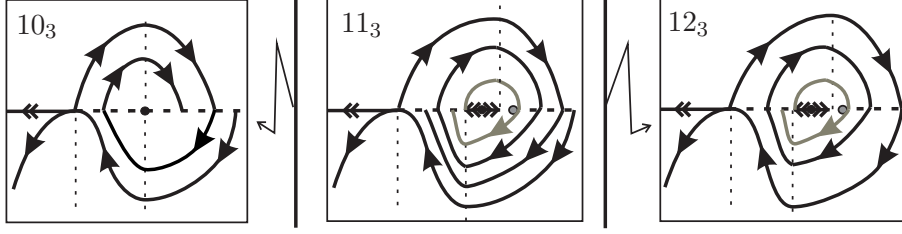
5. PROOF OF THEOREM 3

Proof of Theorem 3. In Case 1₃ we assume that Y presents the behavior Y^- . In Cases 2₃, 3₃ and 4₃ we assume that Y presents the behavior Y^0 . In Cases 5₃ – 19₃ we assume that Y presents the behavior Y^+ .

◊ *Case 1₃*. $\beta < 0$, *Case 2₃*. $\lambda < 0$, *Case 3₃*. $\lambda = 0$, *Case 4₃*. $\lambda > 0$, *Case 5₃*. $\lambda < -\sqrt{\beta}$, *Case 6₃*. $\lambda = -\sqrt{\beta}$, *Case 7₃*. $-\sqrt{\beta} < \lambda < 0$, *Case 8₃*. $\lambda = 0$ and *Case 9₃*. $0 < \lambda < \sqrt{\beta}$: By the choice of the bump function B , these cases are analogous to Cases 1₁, 2₁, 3₁, 4₁, 5₁, 6₁, 7₁, 8₁ and 9₁.

◊ *Case 10₃*. $\lambda = \sqrt{\beta}$: The distribution of the connected components of Σ and the behavior of H are the same as Case 12₂. This case differs from Case 12₂ because, as observed in Subsection 2.1.3, when $\lambda = \sqrt{\beta}$ and $\mu > 0$ canard cycles of Z do not arise (see Figure 10) bifurcating from the non hyperbolic canard cycle Γ of Case 12₃ below. Moreover, the tangential singularity $d = b$ behaves itself like a weak attractor. See Figure 26. There exists a hyperbolic repeller canard cycle Γ of kind III passing through a and c .

◊ *Case 11₃*. $\sqrt{\beta} < \lambda < \sqrt{\beta} - \mu/2$: The points of Σ on the left of a and on (b, d) belong to Σ^e . The points on (a, b) and on the right of d belong to Σ^c . The graph of H is like H-3 of Figure 14. We can prove that $p_1 \in (b, d)$

FIGURE 26. Cases $10_3 - 12_3$.

is a Σ -repeller and r_1 is on the right of d . Since $\varrho_Y(\varrho_X(a)) \in (a, b)$ there exists a point $Q \in (\varrho_Y(\varrho_X(a)), \varrho_Y(d))$ such that $\eta'(Q) = 1$. So there exists a hyperbolic attractor canard cycle Γ , of kind I, passing through Q . See Figure 26. By Lemma 9, in this Hopf Bifurcation a unique canard cycle arises. Moreover, there exists a hyperbolic repeller canard cycle Γ of kind III passing through a and c .

◊ *Case 12_3 .* $\lambda = \sqrt{\beta} - \mu/2$: The configuration on Σ and the graph of H are the same as Case 11_3 . The attractor canard cycle Γ presented in the previous case is persistent. Recall that this canard cycle is born from the bifurcation of Case 10_3 . So, the radius of Γ does not tend to zero when λ tends to $\sqrt{\beta} + \mu/2$. Moreover, it appears a non hyperbolic canard cycle passing through a and c . See Figure 24.

◊ *Case 13_3 .* $\sqrt{\beta} - \mu/2 < \lambda < L_1$, *Case 14_3 .* $\lambda = L_1$, *Case 15_3 .* $L_1 < \lambda < 2\sqrt{\beta} - \mu/2$, *Case 16_3 .* $\lambda = 2\sqrt{\beta} - \mu/2$, *Case 17_3 .* $2\sqrt{\beta} - \mu/2 < \lambda < 3\sqrt{\beta} - \mu$, *Case 18_3 .* $\lambda = 3\sqrt{\beta} - \mu$ and *Case 19_3 .* $\lambda > 3\sqrt{\beta} - \mu$: The analysis of these cases is done in a similar way as Cases 11_1 , 12_1 , 13_1 , 14_1 , 15_1 , 16_1 and 17_1 , respectively.

The bifurcation diagram is illustrated in Figure 25 replacing the number 2 subscript by the number 3. \square

6. PROOF OF THEOREM A

Proof of Theorem A. Since in Equation (1) we can take $\mu \in (-\mu_0, \mu_0)$, from Theorems 1, 2 and 3 we derive that its bifurcation diagram contains all the 55 cases described in Theorems 1, 2 and 3. But some of them are Σ -equivalent and the number of distinct topological behaviors is 23. Moreover, each topological behavior can be represented respectively by the Cases 1_1 , 2_1 , 3_1 , 4_1 , 5_1 , 6_1 , 7_1 , 8_1 , 9_1 , 10_1 , 11_1 , 12_1 , 13_1 , 14_1 , 15_1 , 16_1 , 17_1 , 10_2 , 11_2 , 12_2 , 10_3 , 11_3 and 12_3 .

The full behavior of the three-parameter family of NSDS's expressed by Equation (1) is illustrated in Figure 27 where we consider a sphere around the point $(\lambda, \beta, \mu) = (0, 0, 0)$ with a small ray and so we make a stereographic projection defined on the entire sphere, except the south pole. Still in relation to this figure, the numbers pictured correspond to the occurrence of the cases described in the previous theorems. As expected, the cases 3_1

and 3_2 are not represented in this figure because they are, respectively, the center and the south pole of the sphere. \square

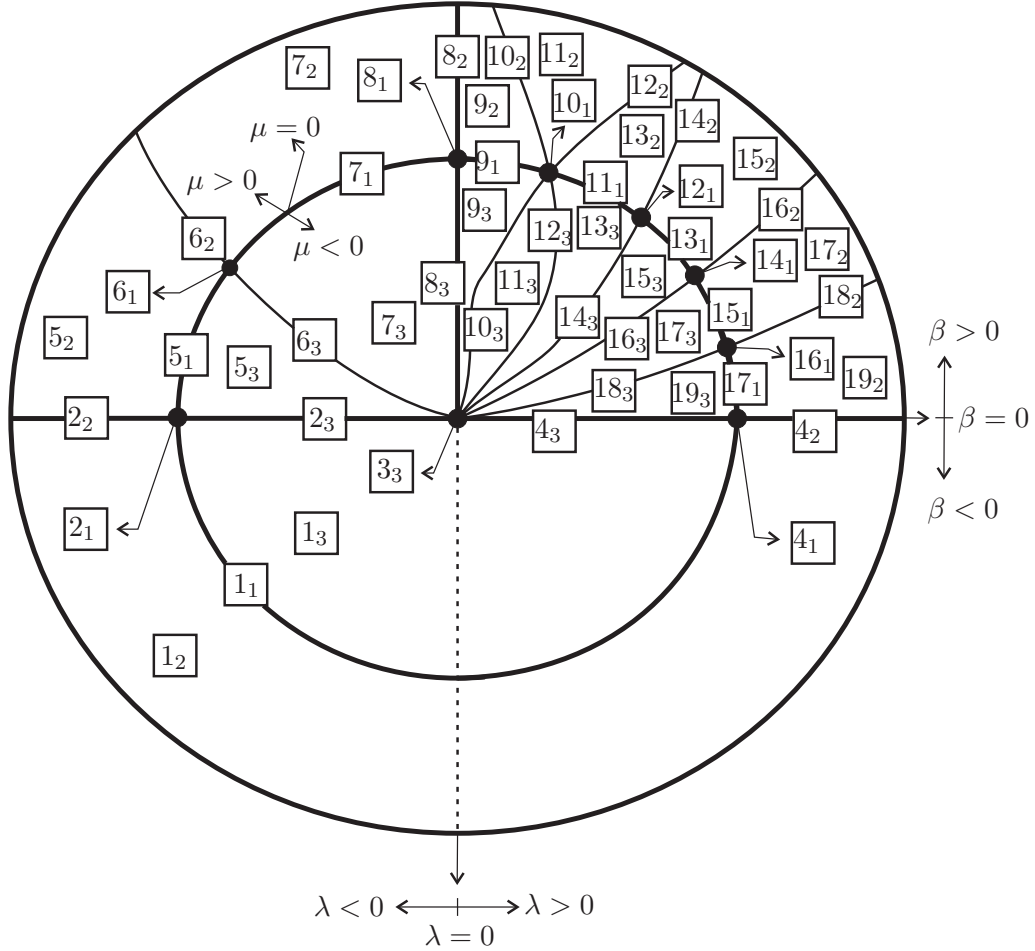


FIGURE 27. Bifurcation diagram of the invisible fold–cusp singularity.

7. PROOF OF THEOREM B

When we consider Equation (3) the function H , given by (8), is constant and equal to 1 independently of the value of μ . Moreover, distinct values of the bump function \tilde{B} (where $\tilde{B} \neq B$) do not produce any topological change in the bifurcation diagram of the singularity. In another words, two parameters are enough to describe the full behavior of this singularity. Observe that, by Proposition 10, we have $\Sigma^f = \emptyset$ and it does not have virtual pseudo equilibria.

Proof of Theorem B. Since X has a unique Σ -fold point which is visible we conclude that canard cycles do not arise. In Case 1_B we assume that Y presents the behavior Y^- . In Cases 2_B , 3_B and 4_B we assume that Y presents the behavior Y^0 . In Cases $5_B - 11_B$ we assume that Y presents the behavior Y^+ .

◇ *Case 1_B .* $\beta < 0$: The points of Σ on the left of d belong to Σ^c and the points on the right of d belong to Σ^e . See Figure 28.

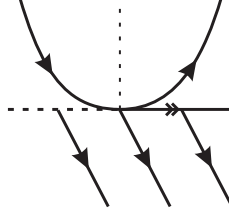


FIGURE 28. Case 1_B .

◇ *Case 2_B .* $\lambda < 0$, *Case 3_B .* $\lambda = 0$ and *Case 4_B .* $\lambda > 0$: The configuration of the connected components of Σ is the same as Case 1_B . Note that, when $\lambda < 0$ (Case 2_B), it appears a tangential singularity $P = (\lambda, 0) \in \Sigma^e$ but Z^Σ is always oriented from the left to the right. These cases are illustrated in Figure 29.

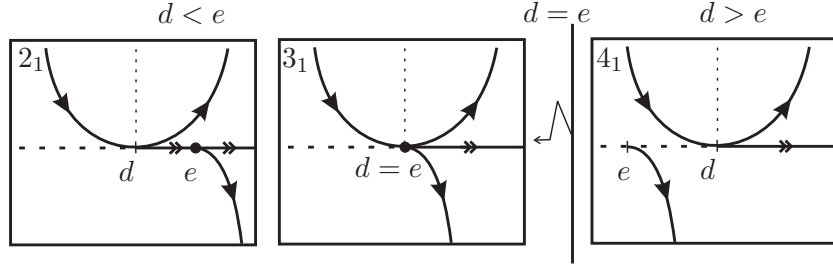


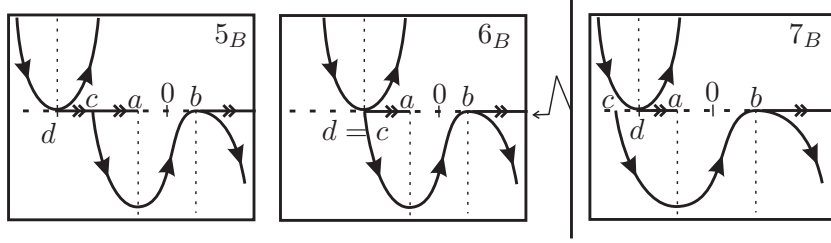
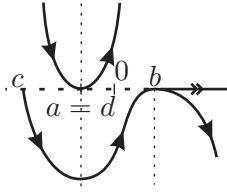
FIGURE 29. Cases $2_B - 4_B$.

◇ *Case 5_B .* $\lambda < -2\sqrt{\beta}$, *Case 6_B .* $\lambda = -2\sqrt{\beta}$ and *Case 7_B .* $-2\sqrt{\beta} < \lambda < -\sqrt{\beta}$: The points of Σ on the right of b and inside the interval (d, a) belong to Σ^e . The points on (a, b) and on the left of d belong to Σ^c . See Figure 30.

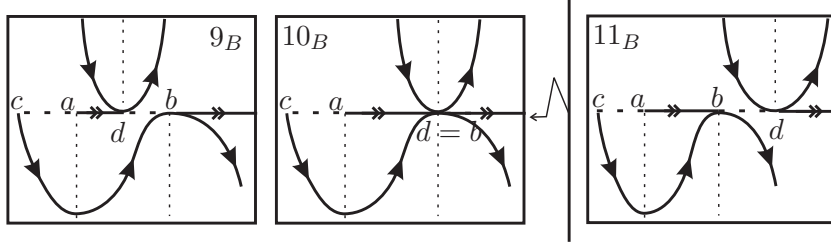
◇ *Case 8_B .* $\lambda = -\sqrt{\beta}$: In this case $a = d$ and the configuration of the connected components of Σ is illustrated in Figure 31.

◇ *Case 9_B .* $-\sqrt{\beta} < \lambda < \sqrt{\beta}$: The points of Σ on the right side of b belong to Σ^e and the points inside the interval (a, d) belong to Σ^s . The points on (d, b) and on the left of a belong to Σ^c . See Figure 32.

◇ *Case 10_B .* $\lambda = \sqrt{\beta}$: In this case $d = b$ and the configuration of the connected components of Σ is illustrated in Figure 32.

FIGURE 30. Cases $5_B - 7_B$.FIGURE 31. Case 8_B .

◇ *Case 11_B . $\lambda > \sqrt{\beta}$:* The points of Σ on the right of d belong to Σ^e and the points inside the interval (a, b) belong to Σ^s . The points on (b, d) and on the left of a belong to Σ^c . See Figure 32.

FIGURE 32. Cases $9_B - 11_B$.

The bifurcation diagram is illustrated in Figure 33. □

8. CONCLUDING REMARKS

The results in Section 12 of [9] were revisited and extended in this paper. The bifurcation diagram of a three-parameter family of NSDS's presenting a fold-cusp singularity is exhibited. In particular it is shown the existence of some new interesting global bifurcations around the standard fold-cusp singularity expressed by (5). Moreover, the simultaneous occurrence of such local and global bifurcations indicates how complex is the behavior of this singularity.

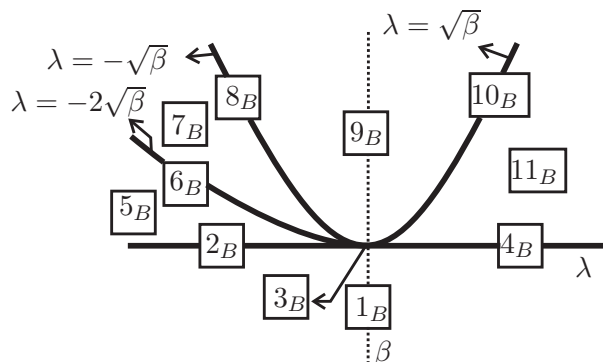


FIGURE 33. Bifurcation Diagram of Theorem B.

Acknowledgments. We would like to thank the referee for helpful comments and suggestions. The first and the third authors are partially supported by a FAPESP-BRAZIL grant 2007/06896-5. The second author was partially supported by FAPESP-BRAZIL grants 2007/08707-5, 2010/18190-2 and 2012/00481-6.

REFERENCES

- [1] A. ANDRONOV AND S. PONTRYAGIN, *Structurally stable systems*, Dokl. Akad. Nauk SSSR **14** (1937), 247–250.
- [2] M. DI BERNARDO, C.J. BUDD, A.R. CHAMPNEYS, P. KOWALCZYK, A.B. NORDMARK, G.O. TOST AND P.T. PIHONEN, *Bifurcations in nonsmooth dynamical systems*, SIAM Rev. **50** (2008), 629–701.
- [3] M. DI BERNARDO, A.R. CHAMPNEYS, S.J. HOGAN, M. HOMER, P. KOWALCZYK, YU.A. KUZNETSOV, A.B. NORDMARK AND P.T. PIHONEN, *Two-parameter discontinuity-induced bifurcations of limit cycles: Classification and open problems*, Internat. J. Bifur. Chaos Appl. Sci. Engrg. **16** (2006), 601–629.
- [4] M. DI BERNARDO, C.J. BUDD, A.R. CHAMPNEYS AND P. KOWALCZYK, *Piecewise-smooth Dynamical Systems – Theory and Applications*, Springer-Verlag (2008).
- [5] C.A. BUZZI, T. DE CARVALHO AND P.R. DA SILVA, *Canard Cycles and Poincaré Index of Non-Smooth Vector Fields on the Plane*, posted in arXiv:1002.4169v1 [math.DS].
- [6] B. COLL, A. GASULL AND R. PROHENS, *Center-focus and isochronous center problems for discontinuous differential equations*, Discrete and Continuous Dynamical Systems **6** (2000), 609–624.
- [7] A.F. FILIPPOV, *Differential Equations with Discontinuous Righthand Sides*, Mathematics and its Applications (Soviet Series), Kluwer Academic Publishers-Dordrecht, 1988.
- [8] P. GLENDINNING, *Non-smooth pitchfork bifurcations*, Discrete and Continuous Dynamical Systems Ser. B **4** (2004), 457–464.
- [9] M. GUARDIA, T.M. SEARA AND M.A. TEIXEIRA, *Generic bifurcations of low codimension of planar Filippov Systems*, Journal of Differential Equations **250** (2011) 1967–2023.

- [10] V. S. KOZLOVA, *Roughness of a Discontinuous System*, Vestnik Moskovskogo Universiteta, Matematika **5** (1984), 16–20.
- [11] YU.A. KUZNETSOV, S. RINALDI AND A. GRAGNANI, *One-Parameter Bifurcations in Planar Filippov Systems*, Int. Journal of Bifurcation and Chaos, **13** (2003), 2157–2188.
- [12] J. SOTOMAYOR, *Generic-one parameter families of vector fields on two-dimensional manifolds*, Inst. Hautes études Sci. Publ. Math., **43** (1974), 5–46.
- [13] M.A. TEIXEIRA, *Generic Bifurcation in Manifolds with Boundary*, Journal of Differential Equations **25** (1977), 65–88.
- [14] M.A. TEIXEIRA, *Generic bifurcation of certain singularities*, Bollettino della Unione Matematica Italiana (5), **16-B** (1979), 238–254.
- [15] M.A. TEIXEIRA, *Generic Singularities of Discontinuous Vector Fields*, An. Ac. Bras. Cienc. **53** (1991), 257–260.
- [16] M.A. TEIXEIRA, *Perturbation Theory for Non-smooth Systems*, Meyers: Encyclopedia of Complexity and Systems Science **152** (2008).
- [17] S.M. VISHIK, *Vector fields near the boundary of a manifold*, Vestnik Moskovskogo Universiteta. Matematika **27** (1972), 21–28.

¹ IBILCE–UNESP, CEP 15054–000, S. J. RIO PRETO, SÃO PAULO, BRAZIL

² FC–UNESP, CEP 17033–360, BAURU, SÃO PAULO, BRAZIL

³ IMECC–UNICAMP, CEP 13081–970, CAMPINAS, SÃO PAULO, BRAZIL

E-mail address: buzzi@ibilce.unesp.br

E-mail address: ti-car@hotmail.com

E-mail address: teixeira@ime.unicamp.br